Materials Chemistry and Physics 267 (2021) 124681

Contents lists available at ScienceDirect

Materials Chemistry and Physics

journal homepage: www.elsevier.com/locate/matchemphys

Tuning grain size, morphology, hardness and magnetic property of electrodeposited nickel with a single multifunctional additive

Aatif Ijaz [a], László Ferenc Kiss [b], A. Levent Demirel [a], Lajos Károly Varga [b], Annamária Mikó [a,*]

[a] Department of Chemistry, Koç University, Rumelifeneri Yolu, Sariyer, Istanbul, 34450, Turkey
[b] Institute for Solid State Physics and Optics, Wigner Research Centre for Physics, Konkoly-Thege Miklós út 29-33, Budapest, 1121, Hungary

HIGHLIGHTS

- Multifunctional Ni films with controlled grain size and roughness are electroplated.
- PEOX serves as a multipurpose additive in Watts bath without incorporating into Ni.
- Nanocrystalline Ni shows preferred crystalline orientation towards (220) plane.
- PEOX concentration controls hardness and tunes magnetic properties of Ni layers.
- The nickel films exhibit high affinity in forming passive oxide layer.

GRAPHICAL ABSTRACT

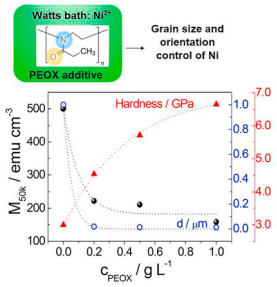

ARTICLE INFO

Keywords:
Nanocrystalline nickel
Electroplating
Oxazoline additive
Grain refinement
Hardness
Magnetic layers

ABSTRACT

The room temperature electrodeposition of high purity, nanocrystalline Ni films prepared in the presence of poly-(2-ethyl-2-oxazoline) (PEOX) as a new multipurpose polymeric additive in Watts bath is presented. The grain size, morphology, hardness and magnetic property of the nickel films were simply tuned by adjusting the concentration of PEOX. Increasing PEOX concentration contributed to grain refinement down to 12.5 nm grain size and crystalline orientation towards (220) planes. The control over the crystalline grain size and the orientation by PEOX concentration allows the preparation of tailor made nickel layers with adjustable physical and chemical properties. The effect of PEOX on the structure is attributed to the high affinity of tertiary amide groups in PEOX for metal surfaces, whereas the incorporation of the macromolecular additive into the nickel layers was prevented. These findings are especially important in emerging applications where smooth, high purity nanocrystalline layers are required. PEOX as a multifunctional additive eliminates the need to use multiple electrolyte additives to obtain a set of desirable properties.

1. Introduction

Electrodeposited nickel layers are extensively used for many applications ranging from decorative coatings to microelectromechanical systems, supercapacitors, micro/nanorobots and magnetic recording media [1–5]. Nickel and nickel alloys are among the leading nanostructured components used for water splitting with the effort to enhance the oxygen evolution reaction activity [6]. Further

* Corresponding author.
E-mail address: amiko@ku.edu.tr (A. Mikó).

https://doi.org/10.1016/j.matchemphys.2021.124681
Received 18 February 2021; Received in revised form 18 April 2021; Accepted 19 April 2021
Available online 23 April 2021

enhancement of the quality of the electroplated Ni layers by controlling the properties such as crystalline grain size, adhesion, texture among others is important for multi-functionality of the coatings in these applications [7,8]. Ni as a coating has excellent adhesion to most of the underlying substrates, high durability and wear resistance, and shows low affinity towards corrosion due to the protective oxide layer on its surface. Ni layers can be electrodeposited from different type of baths, the most common ones containing sulfate, chloride or sulfamate salts. The properties of the nickel layers such as structure, mechanical, optical and magnetic properties can be influenced by the current density applied for electrodeposition as well as with the pH, temperature and composition of the deposition bath [9,10]. The variation of these parameters such as the effect of the substrate on the growth mechanism, morphology, microstructure and magnetic properties of electrodeposited Ni was extensively investigated [11–18].

Watts solution is one of the most widely used bath for the electrodeposition of Ni [19,20] because of its long term stability and ability to operate in the presence of various additives. The most commonly used additives are diols [21], quaternary ammonium salts [20,22], aliphatic alcohols [23], and poly alcohols [24]. These additives contribute to the refinement of grain structure, impart leveling, improve the tensile strength, ductility and act as brighteners [25]. Organic compounds having imine, carbonyl, thioamide and aromatic sulfonate groups are the most frequently used brightening and leveling agents for Ni electrodeposition. They contain lone pair electrons which result in their high affinity to adsorb on metallic surfaces [26].

Fig. 1 shows the chemical structure of two commonly used additive with grain refining effect a) coumarin and b) saccharin, in addition to the chemical structure of c) poly-(2-ethyl-2-oxazoline) (PEOX) used in this work.

The effect of brighteners on the coating morphology was well investigated [22,24,27,28] and shown to shift nickel electrodeposition to a more negative electrode potential. As a result, molecules like saccharin reduced the grain size of the coatings which improved the hardness and decreased the stress in the Ni layers [29–32]. This improvement was attributed to the incorporation of Sulphur atoms at the grain boundaries of the Ni deposits from saccharin [29]. But, at high temperature this caused embrittlement of the deposits and reduced the corrosion resistance [33,34]. Saccharin was concluded to be not enough effective to produce bright coatings; therefore, auxiliary additives were required to improve the brightness of the coatings [22,29].

PEOX is a water soluble, biodegradable, non-toxic, environmentally friendly polymer. The polymeric structure contains carbonyl and amide groups which allow the polymer chains to be adsorbed on the metal surface and influence the structure of the coatings. The grain size of a crystalline metal is strongly dependent on the adatom mobility [26]. Therefore, it is anticipated that a molecule like PEOX (Fig. 1c) containing nitrogen and oxygen atoms with high adsorption affinity should have a strong grain refinement effect similar to that of polyacrylamide [35], together with the advantage of PEOX having low affinity towards hydrolysis and decomposition compared to polyacrylamide.

In this work, PEOX is introduced as a new multipurpose additive for nickel electrodeposition to control the physical and chemical properties of the nickel layers through grain refinement and crystal orientation. The room temperature electrodeposition of Ni layers was systematically studied as a function of PEOX additive concentration to investigate the effect of PEOX concentration on the structure and morphology of the layers. It is demonstrated that the control over the grain size and crystalline orientation of the layers are the key parameters to tune the hardness, reflectance, magnetic property and electrochemical activity which gives flexibility in the design and realization of Ni layers for various applications.

2. Experimental

Nickel coatings were electrodeposited on a copper substrate by applying direct current electrodeposition method using Pt–Ir alloy as an anode. The electrolyte bath was a typical Watts bath with the composition of $NiSO_4{\cdot}6H_2O$ (150 g L^{-1}), $NiCl_2{\cdot}6H_2O$ (65 g L^{-1}), H_3BO_3 (37.5 g L^{-1}) and PEOX (0–1 g L^{-1}) as an additive. All the electrodeposition process was carried out at 23.5 °C and at pH 3 with the stirring rate of 500 rpm. The current density was altered as 10, 30, 50, 70 and 100 mAcm^{-2}. PEOX (Mw. 50,000 g mol^{-1}) and analytical grade nickel sulfate, nickel chloride, boric acid were purchased from Sigma Aldrich. The copper substrates (99.44 wt% purity) were purchased from Cakir Kimya (Turkey). Before the electrodeposition of Ni coatings, the Cu substrates were first washed with deionized water and then with ethanol. The substrates were dried with nitrogen gas flow. After electrochemical deposition of Ni coatings, the samples were rinsed with deionized water and dried in nitrogen gas flow. The thickness of the deposited films was ~20 μm.

The morphology of the electrodeposited Ni coatings was characterized by field emission scanning electron microscope (SEM, Zeiss Ultra Plus). The roughness of the electrodeposited samples was determined by atomic force microscope (AFM, Bruker Dimension) in tapping mode using silicon cantilevers. The average route mean squared surface roughness values were obtained by scanning three different 40 × 40 μm^2 areas on each sample. For magnetic domain structure determination, MFM imaging was done in lift mode using Co–Cr coated cantilevers. MFM images were taken at the same scan height of 40 nm at room temperature.

The reflectance of the Ni coatings was investigated by UV–Vis spectroscopy. The nanoindentation hardness of electrodeposited Ni coatings was measured by mechanical properties microprobe (Agilent G200). A Berkovich diamond tip indenter was used to make 100 mN indentations on ten selected locations of each sample. The reported hardness value is the average of 10 indentation measurements for each sample.

The crystalline structure of the electrodeposited Ni films was investigated by powder X-ray diffraction measurements (XRD, Bruker D8 Advance). Thermo Scientific K-Alpha spectrometer was used to record the XPS spectra. The X-ray source was monochromatized Al-Kα radiation and the charge compensation during the measurements was controlled by flood gun at a vacuum chamber pressure ~2.0 × 10^{-7} mbar. The spectra were referenced to C1s neutral carbon peak binding energy at 284.6 eV. The relative atomic concentration was obtained from the

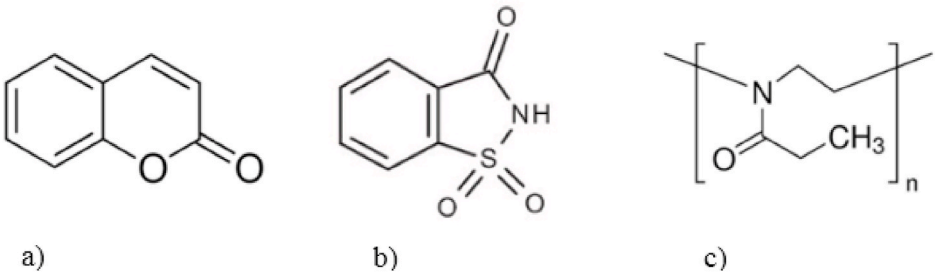

Fig. 1. Chemical structure of a) coumarin, b) saccharin and c) poly-(2-ethyl-2-oxazoline) (PEOX).

deconvoluted core-level spectra.

The electrochemical measurements were performed in a NaCl (0.5 M) solution by using EG&G 272 potentiostat in standard three-electrode cell configurations. The Ni coated Cu substrates was used as a working electrode, Pt–Ir electrode was the counter electrode, and Ag/AgCl in saturated KCl solution served as the reference electrode. Prior to each polarization experiments, open circuit potential (OCP) was monitored. The cyclic polarization curves were obtained by moving to the electrode potential of +100 mV or +130 mV (vs Ag/AgCl in saturated KCl solution) with the scan rate of 5 mVs^{-1}. The corrosion current density and the corrosion potential were obtained from Tafel curves by extrapolating the linear parts. The Tafel plots were registered between −250 mV and +250 mV from the open circuit potential with a scan rate of 0.2 mVs^{-1}.

The magnetic measurements were carried out with the help of a Quantum Design MPMS-5S superconducting interference device (SQUID) in the magnetic field range of $0 \leq H \leq 50$ kOe at $T = 5$ K. The samples together with the substrate were cut into pieces with a geometry of ca. 6.2×6.2 mm^2 which were pressed between the walls of a drinking straw. The magnetization was calculated from the cross section and thickness (20 μm) of the Ni coatings. The magnetization measured at the highest magnetic field (H = 50 kOe) was taken as the saturation magnetization.

3. Results and discussions

3.1. Effect of the additive concentration on the morphology and onset potential of the electrodeposited Ni layers

The effect of the additive concentration on the surface morphology is presented in Fig. 2a–d (and in Supporting Information Fig. S1). All the samples were obtained from Watts bath at room temperature. For the additive-free case, the SEM images depicted Ni coatings with micrometer size pyramidal crystals (800 nm–1500 nm) surrounded by smaller size grains (200–400 nm). Introducing PEOX to the electrolyte bath had a strong grain refinement effect on the surface morphology as shown in Fig. 2b–d for 10 $mAcm^{-2}$ cathodic current density. A closer observation of the 10 $mAcm^{-2}$ samples demonstrated that the pyramid-like nickel crystals with relatively large surface roughness changed to a smooth morphology with few ~20 nm diameter valleys, due to the addition of 0.2 g L^{-1} PEOX (Fig. 2b).

Further increase in the concentration of PEOX to 0.5 and 1.0 g L^{-1} resulted in a smoother and more compact surface morphology with a negligible number of pores. The cathodic current density in the presence of PEOX was altered between 10 and 100 $mAcm^{-2}$. The grain refining effect of PEOX on the surface morphology of the electrodeposited Ni coatings was observed at all investigated current densities, similar to that shown in Fig. 2 at 10 $mAcm^{-2}$. Some cracks were also observed on the samples deposited from additive containing solution indicating the presence of internal stress in the coatings. All additive-free samples showed similar micron-sized pyramidal morphology regardless of the current density, in line with the literature results [36]. Linear sweep voltammogram recorded in Watts bath at room temperature is shown in Fig. 2e. The onset potential for Ni electrodeposition shifted gradually towards the more negative values as PEOX concentration was increased in the electrodeposition bath (Fig. 2f). The steep decrease in the current density with decreasing potential was associated with the deposition of Ni and possibly accompanied by hydrogen evolution reaction.

In PEOX free bath the steep decrease in current density started at −700 mV, shifted to −840 mV at 0.2 g L^{-1} PEOX concentration and to −933 mV at 0.5 g L^{-1} PEOX concentration. The most negative value of −950 mV was observed at 1.0 g L^{-1} PEOX concentration in the electrolyte bath. The gradual shift in the onset potential with increasing additive concentration, as presented in Fig. 2, suggests an inhibited Ni electrodeposition. The monomer of ethyl-2-oxazoline is known to have a high tendency to interact with the metallic surface through the amide dipole of the molecule [37–39]. The adsorption tendency for PEOX chain is even stronger due to connectivity of monomers [40]. The presence of carbonyl and amide groups in PEOX structures enhances the availability of π-electrons for the coordination between the metallic cathode and PEOX molecules [39,41,42]. Therefore, the shift in the onset potential towards a more negative value can be attributed to the adsorption of PEOX molecules on the cathode surface indicating a competition between the PEOX chains and the adatom nickel species reaching the cathode surface. Similarly, this "blocking" effect of the

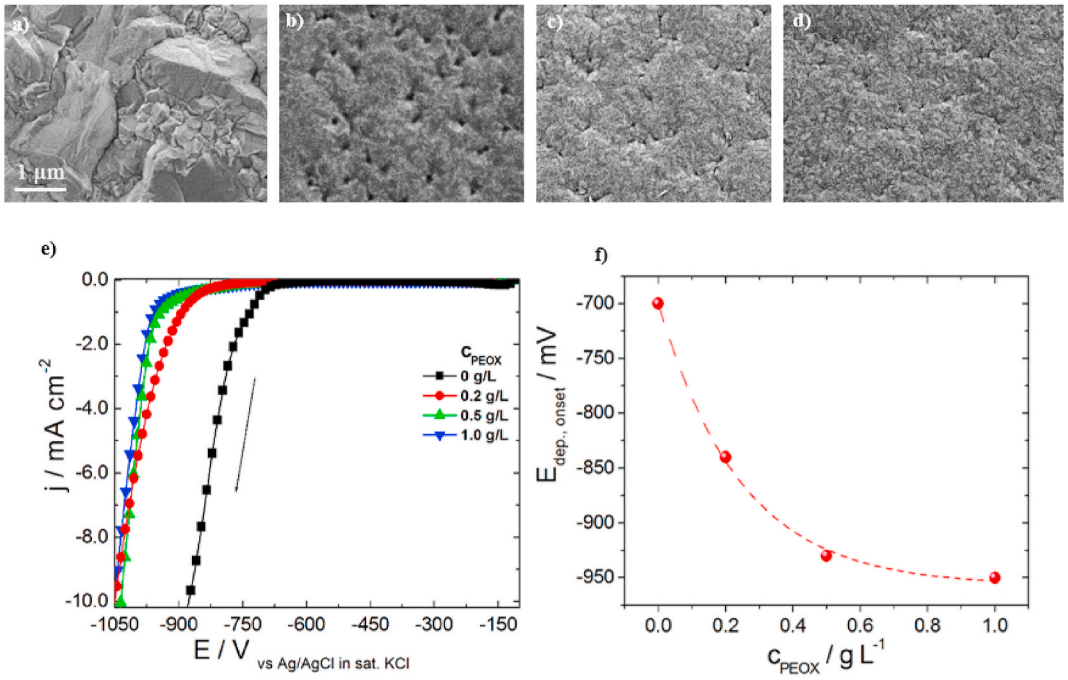

Fig. 2. a-d) SEM images of electrodeposited Ni coatings obtained from Watts bath produced at 10 mA/cm^2 with a) 0 g L^{-1}, b) 0.2 g L^{-1}, c) 0.5 g L^{-1} and d) 1 g L^{-1} PEOX concentration in the bath. The scale bar shown for a) is 1 μm and valid for all of the SEM images, *e)* The cathodic polarization curves recorded in the electrolyte bath at different additive concentrations and f) onset potential of Ni deposition. The dashed line is to guide the eye.

organic compound was observed in the literature for electrolyte baths using typical organic additives [9,19,29,36].

3.2. Effect of additive concentration on the grain size and texture of the nickel coatings

The structure and the grain size of the nickel layers were investigated by powder XRD measurements to understand the effect of PEOX addition in Watts bath on the nickel film formation. Fig. 3 shows the XRD patterns of Ni coatings deposited at 10 mAcm^{-2} from the solution containing varying concentrations of PEOX. The samples showed diffraction peaks at (111), (200) and (220) planes. These results confirm that all nickel deposits are polycrystalline and crystallized in face-centered cubic shape. In the case of additive-free solution, the diffraction peaks of (111) and (200) plane showed higher intensity relative to the (220) plane, typical for electrodeposited nickel layers without preferred orientation. However, after the addition of PEOX in the deposition solution, the diffraction peak of (220) planes became the most dominant in the spectra, indicating a preferred (220) crystal orientation of Ni. Table 1 summarizes the relative texture coefficients calculated from the XRD results of the samples. The calculations were performed according to equation (1) in line with the work of Harris [43].

$$RTC_{(hkl)} = \frac{I_{hkl}/I^{o}_{hkl}}{\frac{1}{n}\sum_{i=1}^{n}\frac{I_{hkl}}{I^{o}_{hkl}}} \times 100\% \quad (1)$$

In equation (1), the corresponding variables are: I_{hkl} = intensity of diffraction planes in the electrodeposited sample; I^{o}_{hkl} = intensity of diffraction planes in bulk Ni powder sample; n = number of planes in the XRD pattern; RTC = relative texture coefficient; hkl = miller indices of planes; I_{hkl} = intensity of diffraction planes in the electrodeposited sample; I^{o}_{hkl} = intensity of diffraction planes in bulk Ni powder sample. The results in Table 1 clearly demonstrated the effect of PEOX on the crystalline growth directionality of electrodeposited Ni samples. An increase in the current density from 10 mAcm^{-2} to 100 mAcm^{-2} did not influence the preferred orientation of the nickel layers, such orientation was only observed in the presence of PEOX polymer in the electrolyte bath. Above 0.2 g L^{-1} additive concentration a plane characteristic for hkl (220) crystalline direction became dominant for each sample. Such a high orientation is possibly induced by the adsorbed PEOX chains on the cathode surface as a result of their slower desorption from the active sites corresponding to hkl (111) and (200) planes compared to hkl (220). In the face-centered cubic lattice the lowest surface energy corresponds to the (220) plane, while (111) plane with the highest surface density of atoms corresponds to the highest surface energy. Easier desorption of the PEOX chains from the lowest energy (220) plane (compared to the other planes) allowed the faster growth of nickel resulting in orientation of the deposited film along [220] direction.

Table 1
Relative texture coefficient and the grain size determined from powder XRD measurements for Ni samples electrodeposited from Watts bath with and without PEOX additive at 10 mAcm^{-2}.

Sample code	c_{PEOX}/ gL^{-1}	hkl (111)	hkl (200)	hkl (220)	Grain size/nm	Lattice strain (Δd/d)
Ni01	0	39.8	220.8	40.0	~1000[a]	n.a.
Ni02	0.2	4.0	8.5	299.2	18.5	3.78·10^{-4}
Ni03	0.5	5.1	8.6	286.1	14.2	3.13·10^{-4}
Ni04	1	4.0	8.4	287.2	12.5	2.36·10^{-4}

[a] The grain size was estimated from SEM images.

The grain size of nickel films electrodeposited from PEOX containing solution was determined using the Hall-Williamson method [44]. The results for 10 mAcm^{-2} cathodic current density are summarized in Table 1. For the additive-free nickel layers, the size was estimated from the SEM images to be in the micrometer range (800–1500 μm). As a result of PEOX addition, a clear decrease to nanometer grain sizes down to ~12–19 nm range was observed in line with the SEM investigations. The grain refinement is related to the control over the adatom mobility due to PEOX adsorption. This was reflected in the higher negative overpotentials recorded with linear sweep voltammetry for PEOX containing solutions compared to the additive-free case (shown in Fig. 2e). This high negative overpotential usually corresponds to enhanced nucleation and the high number of crystal seeds which results in grain refinement compared to the additive-free case [19].

The surface roughness of the electrodeposited Ni coatings was determined by AFM. The 2-dimensional height images of Ni coatings deposited at 10 mAcm^{-2} containing various concentrations of PEOX are shown in Fig. 4. The color intensity of the images shows the surface profile of electrodeposited Ni coatings.

The surface roughness of the Ni coatings has decreased dramatically in the presence of 0.2 g L^{-1} PEOX (sample Ni02) and continued to

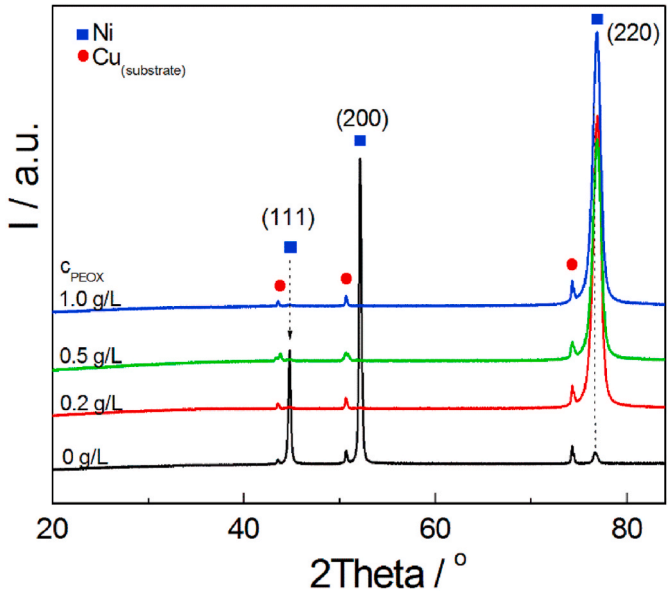

Fig. 3. XRD patterns of Ni electrodeposited at 10 mAcm^{-2} from Watts bath containing different concentrations of PEOX. All the films were prepared at room temperature.

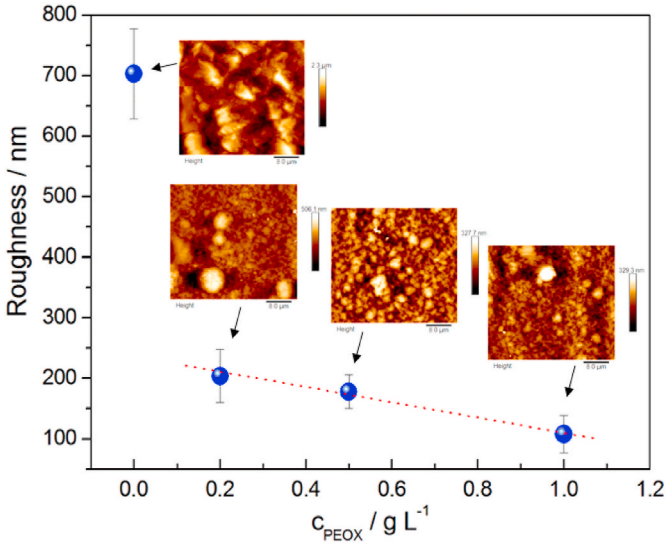

Fig. 4. Surface roughness of electrodeposited Ni coatings obtained from Watts bath containing different concentrations of PEOX at 10 mAcm^{-2} current density. The inserts show AFM height images of the layers. The scale bar is 8 μm.

decrease further with increasing PEOX concentration. A linear decrease in the surface roughness was observed with increasing PEOX concentration which indicates that the surface roughness of nickel layers can simply be controlled by adjusting the PEOX concentration. Similar morphological changes were observed for all the samples coated from electrolyte bath containing PEOX in the investigated deposition current density range, however higher number of cracks were observed when the current density was increased. The relatively high negative onset potential for electrodeposition compared to additive free cases is accompanied with higher hydrogen evolution rate. When the current density increases, the deposition potential also shifts towards more negative potential which causes further increase in hydrogen evolution and results in stress formation. In addition, a clear change in the orientation towards the (220) planes was observed. The combination of these two factors probably contributed to the formation of cracks in the films as shown in Supporting Information Fig. S2. The decrease in surface roughness is due to the grain refinement of Ni coatings by the addition of PEOX into the deposition bath in good agreement with the SEM, XRD, and cathodic linear sweep investigations.

3.3. Composition of the nickel layers

The effect of PEOX on the composition of the nickel layers was investigated by X-ray Photoelectron Spectroscopy measurements.

Fig. 5 shows the XPS survey spectra of a Ni sample deposited at 10 $mAcm^{-2}$ from 1.0 g L^{-1} PEOX concentration. All the measurements were taken after 60 s Ar bombardment of the sample to avoid the signal from the cavity adsorbed PEOX as a residue from the deposition bath and to penetrate under the native oxide layer of Ni developed at atmospheric condition. The surface analysis of electrodeposited films clearly demonstrated a high purity Ni sample (99.9 at% purity). The absence of Nitrogen peak in XPS survey confirmed that PEOX was not incorporated into electrodeposited Ni films. Similarly, all the investigated samples were nitrogen-free indicating that PEOX does not incorporate into the coatings at different PEOX concentrations.

3.4. Effect of the additive concentration on the brightness and hardness of the nickel coatings

The presence of PEOX in deposition solution enhanced the brightness of electrodeposited Ni coatings, as well. The difference in the brightness of the Ni coatings electrodeposited from deposition bath with/without PEOX was clearly apparent. Coatings obtained without any additive at room temperature had a "silky" appearance while the addition of PEOX to the solution resulted in bright coatings at each investigated case. However, the formation of some cracks was also observed. The effect of PEOX on the brightness and reflectance of electrodeposited Ni coatings was determined by UV–Vis spectroscopy. The reflectance of Ni coatings in the visible wavelength range of 400–700 nm is shown in Fig. 6. The addition of PEOX into the Ni deposition bath led to an enhanced degree of reflection. The degree of reflection for the Ni02 sample was 9–14% greater than measured for Ni01 coatings and was further enhanced to 14–16% by increasing the concentration of PEOX to 1 g L^{-1} (Ni04 sample). This improvement in the reflection is attributed to the decrease in the roughness of electrodeposited coatings [45–47].

The coatings exhibited excellent adhesion to the Cu substrate for each deposited sample both for the additive free and PEOX containing solutions. Neither the extensive and repeated bending of the substrate, nor the mechanical scratching allowed the removal of the films.

The nanometer-size grains as well as high (220) crystalline texture induced by the addition of PEOX in Ni deposition bath was reflected in the hardness of the electrodeposited Ni coatings.

Fig. 7 shows the hardness value of Ni samples as a function of the grain sizes. Our experimental results (shown in Fig. 7 as solid circles) showed a clear increase in the hardness with decreasing grain size (d) of the electrodeposited coatings produced from Watts bath with 10 mA/cm^2 cathodic current density at room temperature. The hardness of Ni coatings increased from 3.00 GPa (d ~100 nm; no PEOX; sample Ni01 in Table 1) to 4.53 GPa (d = 18.5 nm; 0.2 g/mL PEOX; sample Ni02 in Table 1) and continued to increase to 6.64 GPa as the PEOX concentration reached to 1 g/mL concentration (d = 12.5 nm; Sample Ni04 in Table 1). Generally, the increase in the hardness of polycrystalline metals with decreasing grain size is explained by the Hall-Petch relationship which states that the strength of a metal depends on the inverse square-root of the grain size, d [48]. Under mechanical deformation, decreasing the grain size increases the contribution of grain boundaries which act as barriers for the movement of dislocations.

However, it was also reported that under a critical grain size, which is estimated to be between 10 and 15 nm for nanocrystalline nickel [49, 50], the hardness tends to decrease, because grain boundary sliding might become more dominant in the deformation mechanism. For electrodeposited Ni films in Watts bath using DC deposition from

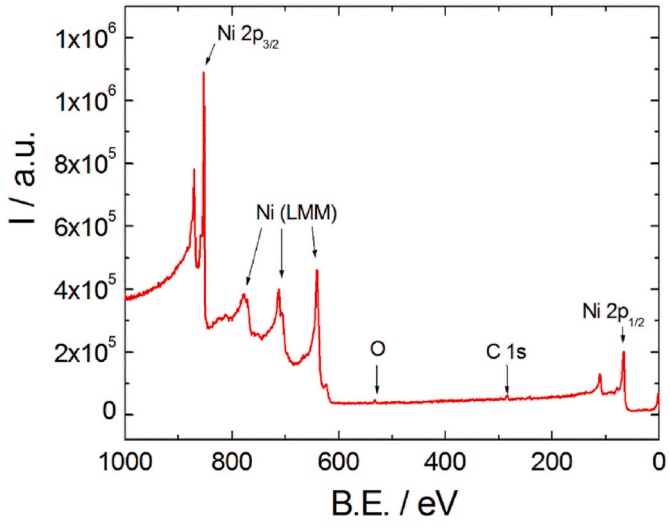

Fig. 5. XPS survey of Ni film electrodeposited at 10 $mAcm^{-2}$ current density from Watts bath at room temperature in the presence of 1.0 g L^{-1} PEOX. The samples were etched with Ar bombardment for 60 s before the measurements were taken.

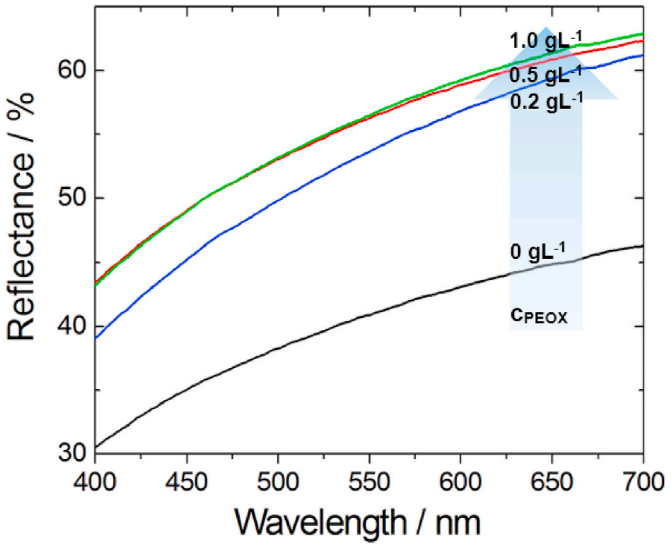

Fig. 6. Effect of PEOX additive on the visible light reflectance of Ni coatings electrodeposited from Watts solution with the cathodic current density of 10 $mAcm^{-2}$ at room temperature.

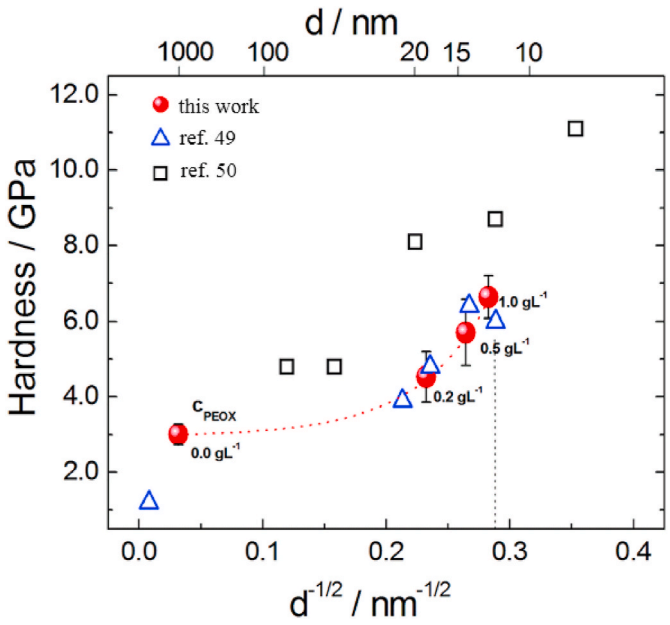

Fig. 7. The effect of grain size as controlled by PEOX concentration on the hardness of nickel samples. Solid circles correspond to the experimental values for Ni samples deposited as described in the text; triangles are from experimental data of reference [49] and squares are experimental values from reference. [50].

Saccharin containing solution, the decrease in the hardness value for the smallest grain size sample at d = 12 nm was attributed to the breakdown of the Hall-Petch hardening [49]. The data of Ref. [49] is shown as triangles in Fig. 7 where the decrease in the hardness value for the smallest grain size sample at d = 12 nm was indicated by vertical dotted line. Hardness in the range of 3.8–6.4 GPa was reported for electrodeposited nickel samples from Saccharin containing solutions [51,52]. In comparison in this work, a monotonic increase in hardness as high as 6.64 GPa was achieved with decreasing grain size down to 12.5 nm (Fig. 7).

We attribute the monotonic increase in hardness and the slightly larger hardness value measured for Ni samples to the fact that PEOX does not incorporate into the coatings. Some Sulphur might be incorporated into the electrodeposited Ni layers from Saccharin containing solution. This might have enhanced grain boundary sliding at grain size of 12 nm resulting in a decrease in the hardness value similar to the work discussed in the literature on non-metallic impurities [53]. In comparison, no indication of grain boundary sliding was observed in this work at grain size of 12.5 nm. Besides, the high relative texture coefficient for (220) orientation for Ni samples in this work can also contribute to the hardness value.

Hardening of high purity Ni particles cured under high-pressure was recently reported with decreasing grain size [50]. The increase in hardness was observed down to a grain size of 3 nm. The data of Ref. 50 covering a grain size range between 8 and 70 nm are shown as squares in Fig. 7. The hardness values were calculated from the reported yield strength values. A monotonous increase of the hardness to 8.7 GPa at 12 nm grain size and 11.1 GPa at 8 nm grain size is seen [50]. The strengthening of the Ni samples having the smallest grain size of 3 nm was attributed to the combined effect of both partial and full dislocation hardening together with suppression of grain boundary plasticity [50]. A monotonous increase in hardness and a hardness value of 6.64 GPa at grain size of 12.5 nm was measured in this work for Ni produced with a simple electrodeposition process at room temperature. In line with Ref. 50, we suggest that the higher purity nickel samples electrodeposited with PEOX additive and having nanocrystalline grain size could extend the breakdown of hardness to smaller grain sizes. The crystal defects in electrodeposited nanograin-sized samples might also contribute to the hardness.

One of the main and fast-developing fields of Ni application arises from its ferromagnetic property as thin-film [54,55]. Main factors such as the film thickness, preparation route, purity, crystal structure, and smoothness influence the magnetic behavior of nickel as well as electron transport properties. Samples electrodeposited with and without additive were compared to investigate the effect of additive present in the deposition bath on the magnetic property of the Ni layers. The thickness of the samples was 20 μm for each investigated case.

3.5. Magnetic properties of the coatings

Fig. 8a shows the magnetic hysteresis as a function of the applied field. A clear difference was observed in the hysteresis and saturation magnetization value (shown in Fig. 8b) of the nickel samples deposited from additive-free and PEOX containing solution. The sample deposited from additive-free solution, shown as an inset in Fig. 8a, had a typical hysteresis characteristic for polycrystalline, micron-sized Ni crystal grain without significant lattice strain. Compared to this sample, the magnetic hysteresis of the films prepared from additive containing bath showed significantly lower (40-16 emucm^{-3}) remanence and was less steeply approaching the saturation magnetization with significantly lower magnetization values. This less steep approach towards magnetic saturation can indicate some crystal defects in the samples as an outcome of nanometer-sized grains and high texture produced in the presence of PEOX additive in the deposition solution. For the sample Ni01, the literature value of the saturation magnetization of bulk Ni (M_s = 512 emucm^{-3}) is obtained, in line with its grain size of ~1 μm deduced from the SEM measurements. The saturation magnetization values shown in Fig. 8b was decreased by 56% for the sample Ni02 (Table 1) and decreased further by a total of 68% with the maximum amount of additive used in the deposition solution. Both the grain size reduced to the nanometer range as well as the tensile lattice strain and the high crystal orientation greatly influences the electronic state of the electrodeposited nickel layer and consequently the strength of the ferromagnetic interaction. Therefore the decrease in the saturation magnetization was attributed to the nano-crystallinity of the samples (d = 12.5–18.5 nm) [56], as well as to the presence of lattice strain modifying the steepness of the approach to magnetic saturation [57,58].

The surface spins of a very small grain become frustrated, resulting in a core-shell structure where only the core will contribute to the magnetization of the grains. Thus, the saturation magnetization of the sample will be reduced. The ability to tune the magnetic property of the pure nickel layers by the additive concentration is much easier compared to the alloying used previously to adjust the saturation magnetization [59].

Fig. 9a shows the change in the saturation magnetization of the samples as a function of the PEOX concentration together with the change in the factors (grain size, lattice strain, texture coefficients) influencing it. A monotonous decrease in the saturation magnetization with PEOX concentration is in line as discussed above with the monotonous decrease in the grain size, lattice strain and with increasing (220) texture in the films. The decrease in the saturation magnetization was large from Ni01 (no additive) to Ni02 which then decreased slowly with increasing PEOX concentration. This trend correlates well with the change in the grain size. These results indicated a possibly more prevalent effect of the crystal structure and morphology on the saturation magnetization for these highly textured layers.

The magnetic domain structure of the electrodeposited Ni films was observed by MFM. A clear difference in the magnetic domain structure was observed between the sample electrodeposited without any PEOX additive (Ni01) and those electrodeposited in the presence of PEOX (Ni02–Ni04). The MFM image of Ni01 is presented in Fig. 9b. Typical striped, but disordered domain structure is seen with few magnetic vortexes. These vortexes possibly form due to the high roughness (~703

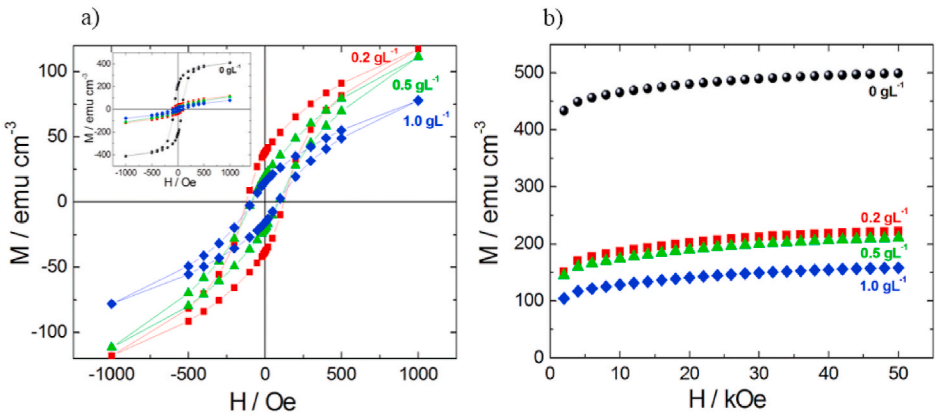

Fig. 8. Hysteresis (a) and magnetization (b) curves for the electrodeposited nickel samples measured at $T = 5$ K.

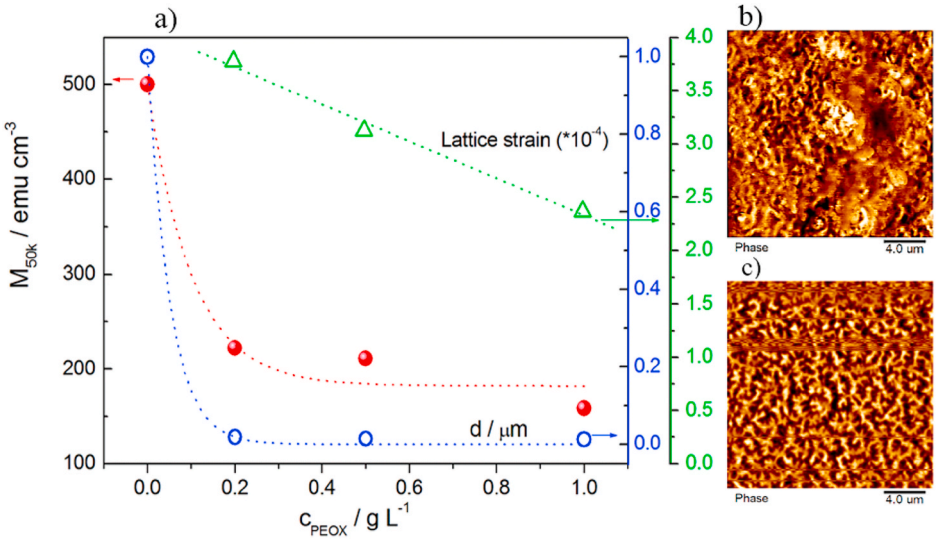

Fig. 9. a) Saturation magnetization, grain size and lattice strain of nickel layers (the dashed lines are shown to guide the eye) as a function of PEOX concentration in the electrolyte bath, b) Magnetic Force Microscopy (MFM) image of nickel sample produced from additive-free bath and c) MFM image of the nickel sample produced in 0.5 g L^{-1} PEOX containing solution. The layers were electrodeposited from Watts bath at room temperature applying 10 $mAcm^{-2}$ cathodic current density.

nm) and pyramid-like crystals of the sample. In line with nearly constant saturation magnetization values for Ni02, Ni03 and Ni04 samples (Fig. 9a), the magnetic domain structure of these samples was similar without any significant differences. Fig. 9c shows the magnetic domain structure of Ni03. A uniformly striped domain structure was observed. The stripes exhibited branching. The uniformity of the domain structure was due to the significantly lower roughness (~178 nm) of Ni03 compared to Ni01. The branching of stripes in the domain structure is possibly the result of the change in the crystalline orientation as well as the effect of the tensile strain in the films, similar to the experimental results in the literature [60].

3.6. Electrochemical behaviour of the coatings

The electronic state, crystal orientation, grain size and the texture do not only influence the magnetic, but also the electrochemical behaviour of the samples. Recently, Ni/NiO_x layers found various applications from robotics [61] to catalysis [62] in which the electrochemical activity and the ability of oxide formation of the nickel layers are critical. The electrochemical behavior of the electrodeposited Ni coatings was investigated in a NaCl (0.5 M) solution. The open-circuit potential (OCP) of electrodeposited Ni coatings was monitored in time. The OCP values of all the samples were in the range of −90 to −490 mV. The most negative open circuit potential was detected for Ni02 sample and gradually shifted towards the more positive value with increasing PEOX additive concentration in line with the lattice strain values in the coatings.

The Tafel curves shown in Fig. 10a were used to determine the corrosion potential (E_{corr}) and corrosion current density (j_{corr}, i.e. reactivity) of the nickel samples according to ASTM-G59 standards and the results are summarized in Table 2. The shift towards the more negative values of the corrosion potential, similar to the open circuit potential values, was observed for the samples Ni02, Ni03, and Ni04 and was accompanied with higher corrosion current density values compared to the sample Ni01. Both the change in the crystalline orientation and the small grain size contribute to higher corrosion current density. Decreasing grain size increases the amount of grain boundaries where the active sites initiate the electrochemical reactions. The variation of the corrosion potential can be the result of several factors including the change in grain size or the change in the lattice strain of the coatings. The shift of the corrosion potential to more positive direction with increasing PEOX concentration is due to the combined effect of both decreasing grain size and decreasing lattice strain. In the case of Ni film without any PEOX additive, the significantly smaller lattice strain is expected to dominate and so the most positive corrosion potential was measured.

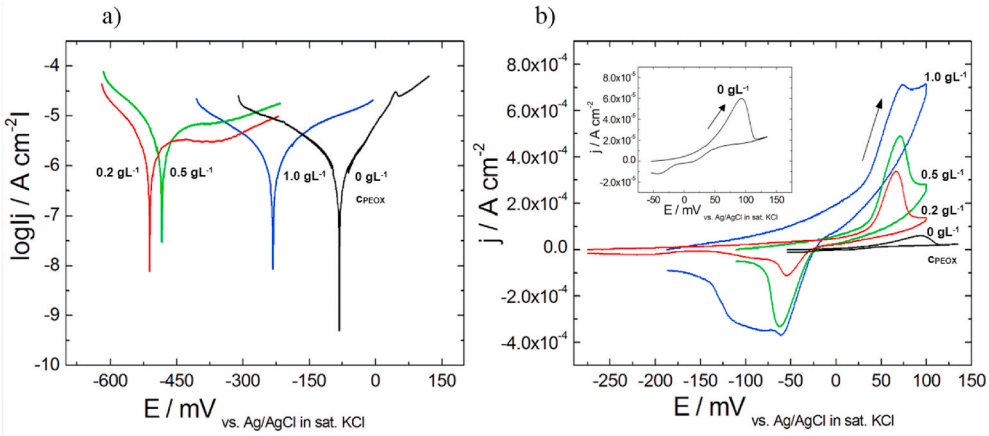

Fig. 10. a) Tafel curves and b) the cyclic voltammograms of electrodeposited Ni coatings in a 0.5 M NaCl solution: sample Ni01 (black), sample Ni02 (red), sample Ni03 (green), and sample Ni04 (blue). The inset shows the enlarged cyclic voltammogram of sample Ni01. (For interpretation of the references to color in this figure legend, the reader is referred to the Web version of this article.)

Table 2
Electrochemical values obtained from Tafel curves and cyclic voltammograms of Ni coatings in NaCl (0.5 M) solution. The values shown in the table correspond to corrosion potential (E_{corr}) and corrosion current density (j_{corr}) from the Tafel curves; peak current (j_p), passivation potential (E_p) and charge (Q) under the forward scan peak curve from cyclic voltammetry measurements.

Sample	j_{corr}/μAcm^{-2}	E_{corr}/mV	j_p/μAcm^{-2}	E_p/mV	Q/μCcm^{-2}
Ni01	0.95	−77.9	52	93.371	3.361
Ni02	2.01	−509.3	334	67.373	20.295
Ni03	4.07	−479.8	485	70.760	26.392
Ni04	1.96	−231.7	708	74.153	58.595

The anodic arc of all samples showed similar oxidation mechanism of Ni to Ni^{2+}. But, a strong diffusion control was observed for Ni02 sample. This diffusion control on the anodic arc gradually decreases for samples Ni03 and Ni04, possibly due to the effect of the decreasing grain size of the layers. The cyclic voltammograms of the Ni films recorded at a scan rate of 5 mVs^{-1} are presented in Fig. 10b. The inset of Fig. 10 shows the cyclic voltammogram of Ni01. All the investigated Ni layers exhibited active-passive behavior in NaCl solution which is typical for Ni samples. The current density increased during the forward scan (indicated with an arrow on Fig. 10b) until the passivation potential (E_p) was reached. The breakdown of the current density then followed indicating the passive layer formation on the Ni. After the breakdown, the current density remained small when the potential was scanned towards more positive values demonstrating that the formed oxide layer is compact and depresses the dissolution rate of the base metal.

The passivation potential for sample Ni02, Ni03 and Ni04 was very close to each other, and the samples were more readily passivating at a lower potential compared to Ni01 sample. This was in the expense of higher current density values as it was reflected in the charge values and passivation current density (Q and j_p, taken from the forward scan) (Table 2). A comparison of the passive current density (j_p) values of the samples showed an increase with decreasing grain size indicating its role in the electrochemical activity. Current density on the backward scan displayed smaller values compared to the forward scan due to the formation of a compact and protective passive layer on Ni. These results clearly show that the small grain size significantly contributes to the electrochemical reaction rate of the samples. It is important to note that the composition and the properties of these films can be adjusted by choosing the proper potential under potentiostatic condition, and perhaps a less aggressive ion instead of Cl^- in the electrolyte, and if needed, by applying heat treatment of the samples.

4. Conclusion

PEOX was successfully introduced into Watts bath as a new multipurpose additive for electrodeposition of Ni coatings at room temperature. The presence of PEOX resulted in (220) orientation to dominate over (111) and (200) crystal orientations in electrodeposited Ni films. SEM and AFM images showed smoother Ni films due the refinement of grain size with the addition of PEOX in the deposition bath. Grain size as low as 12.5 nm was achieved as confirmed by powder XRD measurements. The surface roughness decreased with increasing PEOX additive concentration indicating that the smoothness of nickel layers can simply be controlled by adjusting the PEOX concentration. All the coatings had good adhesion, whereas the brightness was increased with the grain refinement and decreasing surface roughness due to PEOX addition. XPS results confirmed that high purity coatings can be deposited without any incorporation of PEOX into the Ni films. The hardness of the layers improved from 3.00 GPa to 6.64 GPa with the addition of PEOX to the deposition bath. Moreover, a breakdown of Hall-Petch relation was not observed at the smallest grain size of 12.5 nm which we attribute to the fact that PEOX does not incorporate into the coatings. This suggests that the increase in the hardness of polycrystalline metals with decreasing grain size according to Hall-Petch relation can be extended to smaller grain sizes for electrodeposited coatings. A significant decrease was recorded in the saturation magnetization of the nanocrystalline layers. This change was connected to possibly more prevalent effect of the crystal size of the layers. The refinement of grains and decrease in the internal strain of Ni coatings was reflected in the electrochemical property of the layers. The electrochemical investigations demonstrated the shift of the corrosion potential and open circuit potential to more negative potential value with increasing lattice strain in the films. The electrochemical reaction rate increased with the addition of PEOX to the deposition solution due to the grain refinement in the coatings. The electrochemical reaction rate was found to be more sensitive to the grain refinement, whereas corrosion potential and open circuit values were shifted with the variation of the lattice strain. For each investigated case high affinity to passive layer formation was observed. All these results show the effectiveness of PEOX as a multipurpose additive for the electrodeposition of multifunctional Ni films having significant potential to be used in various applications.

CRediT authorship contribution statement

Aatif Ijaz: Conceptualization, Methodology, Investigation, Validation, Formal analysis, Writing – original draft, Writing – review & editing. **László Ferenc Kiss:** Investigation, Writing – review & editing,

Validation, Formal analysis. **A. Levent Demirel:** Writing – review & editing, Resources, Validation, Formal analysis. **Lajos Károly Varga:** Investigation, Writing – review & editing. **Annamária Mikó:** Conceptualization, Methodology, Validation, Formal analysis, Investigation, Writing – original draft, Writing – review & editing, Visualization.

Declaration of competing interest

The authors declare that they have no known competing financial interests or personal relationships that could have appeared to influence the work reported in this paper.

Acknowledgments

The authors thank for the support of Koç University Surface Science and Technology Center (KUYTAM) and Koç University Boron and Advanced Chemicals Application and Research Center (KUBAM). Special thanks for Dr. Zerrin Altintaş for the help in the powder XRD measurements, for Dr. Amir Motallebzadeh for the hardness measurements and Dr. Bariş Yağci for his support in SEM investigations and XPS measurements.

Appendix A. Supplementary data

Supplementary data to this article can be found online at https://doi.org/10.1016/j.matchemphys.2021.124681.

References

[1] R. Oriňáková, A. Turoňová, D. Kladeková, M. Gálová, R.M. Smith, Recent developments in the electrodeposition of nickel and some nickel-based alloys, J. Appl. Electrochem. 36 (9) (2006) 957–972, https://doi.org/10.1007/s10800-006-9162-7.

[2] D. Landolt, Electrodeposition science and technology in the last quarter of the twentieth century, J. Electrochem. Soc. 149 (3) (2002) S9–S20, https://doi.org/10.1149/1.1469028.

[3] P.C. Andricacos, N. Robertson, Future directions in electroplated materials for thin-film recording heads, IBM J. Res. Dev. 42 (5) (1998) 671–680, https://doi.org/10.1147/rd.425.0671.

[4] L. Liu, H. Zhao, Y. Wang, Y. Fang, J. Xie, Y. Lei, Evaluating the role of nanostructured current collectors in energy storage capability of supercapacitor electrodes with thick electroactive materials layers, Adv. Funct. Mater. 28 (6) (2018) 1705107, https://doi.org/10.1002/adfm.201705107.

[5] J. Yan, S. Li, B. Lan, Y. Wu, P.S. Lee, Rational design of nanostructured electrode materials toward multifunctional supercapacitors, Adv. Funct. Mater. 30 (2) (2020) 1902564, https://doi.org/10.1002/adfm.201902564.

[6] X. Wang, W. Li, D. Xiong, D.Y. Petrovykh, L. Liu, Bifunctional nickel phosphide nanocatalysts supported on carbon fiber paper for highly efficient and stable overall water splitting, Adv. Funct. Mater. 26 (23) (2016) 4067–4077, https://doi.org/10.1002/adfm.201505509.

[7] Y. Lin, J. Pan, H.F. Zhou, H.J. Gao, Y. Li, Mechanical properties and optimal grain size distribution profile of gradient grained nickel, Acta Mater. 153 (2018) 279–289, https://doi.org/10.1016/j.actamat.2018.04.065.

[8] K. Schüler, B. Philippi, M. Weinmann, V.M. Marx, H. Vehoff, Effects of processing on texture, internal stresses and mechanical properties during the pulsed electrodeposition of nanocrystalline and ultrafine-grained nickel, Acta Mater. 61 (11) (2013) 3945–3955, https://doi.org/10.1016/j.actamat.2013.03.008.

[9] H. Abdel-Rahman, A. Harfoush, A. Moustafa, Effect of new diamine additives on rate and qualities of nickel deposition, Transact. IMF 91 (1) (2013) 32–43, https://doi.org/10.1179/00202967122.00000000061.

[10] Y. Wang, C. Yang, J. He, W. Wang, N. Mitsuzak, Z. Chen, Effects of choline chloride on electrodeposited Ni coating from a Watts-type bath, Appl. Surf. Sci. 372 (2016) 1–6, https://doi.org/10.1016/j.apsusc.2016.01.182.

[11] M. Boubatra, A. Azizi, G. Schmerber, A. Dinia, The influence of pH electrolyte on the electrochemical deposition and properties of nickel thin films, Ionics 18 (4) (2012) 425–432, https://doi.org/10.1007/s11581-011-0642-3.

[12] M. Boubatra, A. Azizi, G. Schmerber, A. Dinia, Morphology, structure, and magnetic properties of electrodeposited Ni films obtained from different pH solutions, J. Mater. Sci. Mater. Electron. 22 (12) (2011) 1804, https://doi.org/10.1007/s10854-011-0366-1.

[13] P. Li, N. Wang, R. Wang, Flower-like nickel nanocrystals: facile synthesis, shape evolution, and their magnetic properties, Eur. J. Inorg. Chem. 2010 15 (2010) 2261–2265, https://doi.org/10.1002/ejic.201000070.

[14] K. Hedayati, G. Nabiyouni, Surface roughness analysis and magnetic property studies of nickel thin films electrodeposited onto rotating disc electrodes, Appl. Phys. A 116 (4) (2014) 1605–1612, https://doi.org/10.1007/s00339-014-8288-4.

[15] J. Ma, J. Zhang, C. Liu, K. Chen, New insight in magnetic saturation behavior of nickel hierarchical structures, Phys. Lett. 381 (35) (2017) 2973–2977, https://doi.org/10.1016/j.physleta.2017.07.021.

[16] T. Kacel, A. Guittoum, M. Hemmous, E. Dirican, R. Öksüzoglu, A. Azizi, A. Laggoun, M. Zergoug, Effect of thickness on the structural, microstructural, electrical and magnetic properties of Ni films elaborated by pulsed electrodeposition on Si substrate, Surf. Rev. Lett. 25 (2) (2018) 1850058, https://doi.org/10.1142/S0218625X18500580.

[17] A.Y. Samardak, V.S. Pechnikov, E.V. Sukovatitsina, A.S. Samardak, A.V. Ognev, L. A. Chebotkevich, H. Mahdizadeh, A. Akbari, F. Nasirpouri, Temperature dependence of magnetic saturation in electrodeposited nanocrystalline nickel films, solid state phenomena, Trans. Tech. Publ. (2014) 292–297. https://doi.org/10.4028/www.scientific.net/SSP.215.292.

[18] H. Chiriac, The substrate influence on the magnetization of nickel electrodeposited thin films, Thin Solid Films 8 (5) (1971) 345–352, https://doi.org/10.1016/0040-6090(71)90082-4.

[19] Y.J. Li Y, X. Huang, Effect of saccharin on the process and properties of nickel electrodeposition from sulfate electrolyte, Int. J. Metall. Mater. Eng. 2 (2016) 123, https://doi.org/10.15344/2455-2372/2016/123.

[20] A. Ciszewski, S. Posluszny, G. Milczarek, M. Baraniak, Effects of saccharin and quaternary ammonium chlorides on the electrodeposition of nickel from a Watts-type electrolyte, Surf. Coating. Technol. 183 (2–3) (2004) 127–133, https://doi.org/10.1016/j.surfcoat.2003.09.054.

[21] T. Sakamoto, K. Azumi, H. Tachikawa, K. Iokibe, M. Seo, N. Uchida, Y. Kagaya, Effects of 2-buthyne-1, 4-diol additive on electrodeposited Ni films from a Watts-type bath, Electrochim. Acta 55 (28) (2010) 8570–8578, https://doi.org/10.1016/j.electacta.2010.07.031.

[22] E. Sezer, B. Ustamehmetoğlu, R. Katırcı, Effects of a N, N-dimethyl-N-2-propenyl-2-propene-1-ammonium chloride-2-propenamide copolymer on bright nickel plating, Surf. Coating. Technol. 213 (2012) 253–263, https://doi.org/10.1016/j.surfcoat.2012.10.057.

[23] Y. Nakamura, N. Kaneko, M. Watanabe, H. Nezu, Effects of saccharin and aliphatic alcohols on the electrocrystallization of nickel, J. Appl. Electrochem. 24 (3) (1994) 227–232, https://doi.org/10.1007/BF00242888.

[24] E.M. Oliveira, G.A. Finazzi, I.A. Carlos, Influence of glycerol, mannitol and sorbitol on electrodeposition of nickel from a Watts bath and on the nickel film morphology, Surf. Coating. Technol. 200 (20) (2006) 5978–5985, https://doi.org/10.1016/j.surfcoat.2005.09.013.

[25] G.A. Di, Bari, electrodeposition of nickel, Moder. Electroplat. 5 (2000) 79–114, https://doi.org/10.1002/9780470602638.ch3.

[26] X. Shi, R.Q. Zhang, C. Minot, K. Hermann, M.A. Van Hove, W. Wang, N. Lin, Complex molecules on a flat metal surface: large distortions induced by chemisorption can make physisorption energetically more favorable, J. Phys. Chem. Lett. 1 (19) (2010) 2974–2979, https://doi.org/10.1021/jz1011753.

[27] T. Mimani, S.M. Mayanna, N. Munichandraiah, Influence of additives on the electrodeposition of nickel from a Watts bath: a cyclic voltammetric study, J. Appl. Electrochem. 23 (4) (1993) 339–345, https://doi.org/10.1007/BF00296689.

[28] L. Yuan, J. Hu, G. Chang, J. Tang, X. Ji, S. Liu, The contribution of heteroatoms in amide derivatives with an identical structure on nickel electrodeposits, J. Electrochem. Soc. 166 (10) (2019) D381–D388, https://doi.org/10.1149/2.0531910jes.

[29] M. Zheng, R. Hilty, The synergic impact of Saccharin and 2-butyne 1, 4 diol on the electrodeposition of nanocrystalline NiW alloy, ECS Transact. 25 (41) (2010) 117–123, https://doi.org/10.1149/1.3422505.

[30] T. Kolonits, P. Jenei, L. Péter, I. Bakonyi, Z. Czigány, J. Gubicza, Effect of bath additives on the microstructure, lattice defect density and hardness of electrodeposited nanocrystalline Ni films, Surf. Coating. Technol. 349 (2018) 611–621, https://doi.org/10.1016/j.surfcoat.2018.06.052.

[31] A. Rashidi, A. Amadeh, The effect of saccharin addition and bath temperature on the grain size of nanocrystalline nickel coatings, Surf. Coating. Technol. 204 (3) (2009) 353–358, https://doi.org/10.1016/j.surfcoat.2009.07.036.

[32] N.P. Wasekar, P. Haridoss, S. Seshadri, G. Sundararajan, Influence of mode of electrodeposition, current density and saccharin on the microstructure and hardness of electrodeposited nanocrystalline nickel coatings, Surf. Coating. Technol. 291 (2016) 130–140, https://doi.org/10.1016/j.surfcoat.2016.02.024.

[33] J.R. Davis, Nickel, cobalt, and their alloys, ASM Int. (2000), https://doi.org/10.1361/ncta2000p003.

[34] J.E. Darnbrough, P.E.J. Flewitt, Growth of abnormal planar faceted grains in nanocrystalline nickel containing impurity sulphur, Acta Mater. 79 (2014) 421–433, https://doi.org/10.1016/j.actamat.2014.05.059.

[35] L. Ding, X. Fan, J. Du, Z. Liu, C. Tao, Influence of three N-based auxiliary additives during the electrodeposition of manganese, Int. J. Miner. Process. 130 (2014) 34–41, https://doi.org/10.1016/j.minpro.2014.05.008.

[36] F. Yang, W. Tian, H. Nakano, H. Tsuji, S. Oue, H. Fukushima, Effect of current density and organic additives on the texture and hardness of Ni electrodeposited from sulfamate and Watt's solutions, Mater. Trans. 51 (5) (2010) 948–956, https://doi.org/10.2320/matertrans.M2009361.

[37] A.B. Mayer, R.W. Johnson, S.H. Hausner, J.E. Mark, Colloidal Silver Nanoparticles Protected by Water-Solublenonionic Polymers and "Soft" Polyacids, (1999), doi: 10.1081/MA-100101606.

[38] H. Huang, X. Ni, G. Loy, C. Chew, K. Tan, F. Loh, J. Deng, G. Xu, Photochemical formation of silver nanoparticles in poly (N-vinylpyrrolidone), Langmuir 12 (4) (1996) 909–912, https://doi.org/10.1021/la950435d.

[39] D. Malina, A. Sobczak-Kupiec, Z. Wzorek, Z. Kowalski, Silver nanoparticles synthesis with different concentrations of polyvinylpyrrolidone, Digest J. Nanomater. & Biostruct. (DJNB) 7 (4) (2012).

[40] S. Hendessi, P.T. Güner, A. Miko, A.L. Demirel, Hydrogen bonded multilayers of poly (2-ethyl-2-oxazoline) stabilized silver nanoparticles and tannic acid, Eur. Polym. J. 88 (2017) 666–678, https://doi.org/10.1016/j.eurpolymj.2016.10.039.
[41] G. Golestani, M. Shahidi, D. Ghazanfari, Electrochemical evaluation of antibacterial drugs as environment-friendly inhibitors for corrosion of carbon steel in HCl solution, Appl. Surf. Sci. 308 (2014) 347–362, https://doi.org/10.1016/j.apsusc.2014.04.172.
[42] N. Velazquez-Torres, H. Martinez, J. Porcayo-Calderon, E. Vazquez-Velez, J. Gonzalez-Rodriguez, L. Martinez-Gomez, Use of an amide-type corrosion inhibitor synthesized from the coffee bagasse oil on the corrosion of Cu in NaCl, Green Chem. Lett. Rev. 11 (1) (2018) 1–11, https://doi.org/10.1080/17518253.2017.1404645.
[43] G. Harris, X. Quantitative measurement of preferred orientation in rolled uranium bars, the London, Edinburgh, and Dublin, Philos. Magaz. J. Sci. 43 (336) (1952) 113–123, https://doi.org/10.1080/14786440108520972.
[44] B.D. Cullity, Elements of X-Ray Diffraction, Addison-Wesley Publishing1956.
[45] N. Nikolić, Z. Rakočević, K. Popov, Reflection and structural analyses of mirror-bright metal coatings, J. Solid State Electrochem. 8 (8) (2004) 526–531, https://doi.org/10.1007/s10008-003-0467-8.
[46] N. Nikolić, Z.L. Rakočević, D.R. Đurović, K.I. Popov, Reflection and structural characteristics of semi-bright and mirror bright nickel coatings, J. Serb. Chem. Soc. 67 (6) (2002) 437–443, https://doi.org/10.2298/JSC0206437N.
[47] E.P. Schmitz, S.P. Quinaia, J.R. Garcia, C.K. de Andrade, M.C. Lopes, Influence of commercial organic additives on the nickel electroplating, Int. J. Electrochem. Sci 11 (2016) 983–997, https://doi.org/10.5923/j.jlce.20180604.08.
[48] Z.C. Cordero, B.E. Knight, C.A. Schuh, Six decades of the Hall–Petch effect–a survey of grain-size strengthening studies on pure metals, Int. Mater. Rev. 61 (8) (2016) 495–512, https://doi.org/10.1080/09506608.2016.1191808.
[49] C. Schuh, T. Nieh, T. Yamasaki, Hall–Petch breakdown manifested in abrasive wear resistance of nanocrystalline nickel, Scripta Mater. 46 (10) (2002) 735–740, https://doi.org/10.1016/S1359-6462(02)00062-3.
[50] X. Zhou, Z. Feng, L. Zhu, J. Xu, L. Miyagi, H. Dong, H. Sheng, Y. Wang, Q. Li, Y. Ma, High-pressure strengthening in ultrafine-grained metals, Nature 579 (7797) (2020) 67–72, https://doi.org/10.1038/s41586-020-2036-z.
[51] S.H.Z. Shirazi, M. Bahrololoom, M. Shariat, The role of functional groups of saccharin in electrodeposition of nanocrystalline nickel, Surf. Eng. Appl. Electrochem. 52 (5) (2016) 434–442, https://doi.org/10.3103/S1068375516050112.
[52] R. Riastuti, A. Rifki, F. Herdino, C. Ramadini, S.T. Siallagan, Effect of saccharin as additive in nickel electroplating on SPCC steel, AIP Conference Proceedings, AIP Publishing, 2018, p. 020012, doi:10.1063/1.5080031.
[53] C.J. Marvel, J.A. Smeltzer, B.C. Hornbuckle, K.A. Darling, M.P. Harmer, On the reduction and effect of non-metallic impurities in mechanically alloyed nanocrystalline Ni-W alloys, Acta Mater. 200 (2020) 12–23, https://doi.org/10.1016/j.actamat.2020.08.083.
[54] A. Hirohata, K. Yamada, Y. Nakatani, L. Prejbeanu, B. Diény, P. Pirro, B. Hillebrands, Review on spintronics: principles and device applications, J. Magn. Magn Mater. (2020) 166711, https://doi.org/10.1016/j.jmmm.2020.166711.
[55] H. Ibach, C. Schneider, Magnon dispersion in Ni/Co multilayers grown on Cu (100), Phys. Rev. B 99 (18) (2019) 184406, https://doi.org/10.1103/PhysRevB.99.184406.
[56] H. Zhang, G. Wu, X. Chen, X. Qiu, Synthesis and magnetic properties of nickel nanocrystals, Mater. Res. Bull. 41 (3) (2006) 495–501, https://doi.org/10.1016/j.materresbull.2005.09.019.
[57] D.-L. Hou, X.-F. Nie, H.-L. Luo, Magnetic anisotropy and coercivity of ultrafine iron particles, J. Magn. Magn Mater. 188 (1–2) (1998) 169–172, https://doi.org/10.1016/S0304-8853(98)00170-X.
[58] J. Friedel, Dislocations: International Series of Monographs on Solid State Physics, Elsevier2013.
[59] E. Pellicer, A. Varea, S. Pané, B.J. Nelson, E. Menéndez, M. Estrader, S. Surinach, M.D. Baró, J. Nogués, J. Sort, Nanocrystalline electroplated Cu–Ni: metallic thin films with enhanced mechanical properties and tunable magnetic behavior, Adv. Funct. Mater. 20 (6) (2010) 983–991, https://doi.org/10.1002/adfm.200901732.
[60] R. Bozorth, Magnetic domain patterns, J. Phys. Radium 12 (3) (1951) 308–321, https://doi.org/10.1051/jphysrad:01951001203030800.
[61] K. Kwan, S. Li, N. Hau, W.-D. Li, S. Feng, A.H. Ngan, Light-stimulated actuators based on nickel hydroxide-oxyhydroxide, Sci. Robot. 3 (18) (2018), https://doi.org/10.1126/scirobotics.aat4051.
[62] M.S. Alnarabiji, O. Tantawi, A. Ramli, N.A.M. Zabidi, O.B. Ghanem, B. Abdullah, Comprehensive review of structured binary Ni-NiO catalyst: synthesis, characterization and applications, Renew. Sustain. Energy Rev. 114 (2019) 109326, https://doi.org/10.1016/j.rser.2019.109326.